Transient-Reinforced Tunnel Coordinated Control of Underactuated Marine Surface Vehicles With Actuator Faults

Wentao Wu, *Graduate Student Member, IEEE*, Ruihang Ji, *Member, IEEE*, Weidong Zhang, *Senior Member, IEEE*, and Yibo Zhang, *Member, IEEE*

***Abstract*— This paper is concerned with a performance-prescribed coordinated control problem of multiple underactuated marine surface vehicles (MSVs) subject to internal uncertainties, external disturbances, and actuator faults. An echo state network-based (ESN-based) transient-reinforced tunnel coordinated control method is proposed for underactuated MSVs with prescribed performance metrics. Specifically, a graph-based trajectory generator is designed to generate reference signals for various application scenarios. In the guidance loop, a tunnel prescribed performance (TPP) is established to characterize the position and heading coordination metrics of underactuated MSVs. With the TPP-based equivalent transformation, the tunnel guidance laws are devised by an underactuation guidance principle. In the control loop, an ESN-based neural estimator is constructed to identify unknown kinetics consisting of internal uncertainties, external disturbances, and actuator faults. Utilizing the estimated information, the ESN-based surge and yaw control laws are presented. The proposed closed-loop system is proven to be input-to-state stable via the theoretical analysis, and position and heading tracking errors can evolve within TPP constraints regardless of actuator faults. Finally, comparison simulation results are employed to verify the effectiveness and superiority of the proposed method.**

***Index Terms*— Underactuated marine surface vehicles, coordination control, tunnel prescribed performance, neural estimator, actuator faults.**

Manuscript received 19 December 2022; revised 12 April 2023, 5 June 2023, 28 June 2023, and 8 August 2023; accepted 13 September 2023. This work was supported in part by the National Key Research and Development Program of China under Grant 2022ZD0119900 and Grant 2022ZD0119903, in part by the Shanghai Science and Technology Program under Grant 22015810300, in part by the Hainan Province Science and Technology Special Fund under Grant ZDYF2021GXJS041, in part by the National Natural Science Foundation of China under Grant U2141234 and Grant 52201369, in part by the Hainan Special Ph.D. Scientific Research Foundation of Sanya Yazhou Bay Science and Technology City under Grant HSPHDSRF-2022-01-007, in part by the China Post-Doctoral Science Foundation under Grant 2022M722053, and in part by the Oceanic Interdisciplinary Program of Shanghai Jiao Tong University under Grant SL2022PT112. The Associate Editor for this article was Y. Wang. *(Corresponding authors: Weidong Zhang; Yibo Zhang.)*

Wentao Wu is with the Department of Automation, Shanghai Jiao Tong University, Shanghai 200240, China, and also with SJTU Sanya Yazhou Bay Institute of Deepsea Science and Technology, Sanya, Hainan 572024, China (e-mail: wentao-wu@sjtu.edu.cn).

Ruihang Ji is with the Department of Electrical and Computer Engineering, National University of Singapore, Singapore 117576 (e-mail: jiruihang@nus.edu.sg).

Weidong Zhang and Yibo Zhang are with the Department of Automation, Shanghai Jiao Tong University, Shanghai 200240, China (e-mail: wdzhang@sjtu.edu.cn; zhang297@sjtu.edu.cn).

Digital Object Identifier 10.1109/TITS.2023.3324346

I. Introduction

INSPIRED by biological behavior in nature, coordination control of marine surface vehicles (MSVs) has attracted increasing attention and interest from research institutes and communities [1], [2], [3], [4], [5], [6], [7]. The coordination control aims to achieve a desired collaborative behavior of MSVs by interacting with neighbors, such as consensus [8], [9], containment [10], [11], flocking [12], [13], formation [14], [15], and so on. As marine missions have more diversity, higher requirements are placed on transient and state-steady metrics of coordination performance for the multi-vehicle system [16], [17].

In recent years, several research results have presented the prescribed performance control (PPC) methods to improve the control performance of MSVs [18], [19], [20], [21], [22], [23], [24], [25], [26]. Specifically, in [18], an adaptive output-feedback performance-guaranteed trajectory tracking control method is investigated, where a high gain observer is constructed to estimate unavailable velocities. In [19], full-state and output feedback adaptive neural network (NN) controllers are developed for one MSV to track a given trajectory with predefined transient performance. In [20], an adaptive neural learning control with predefined performance is proposed for accurately unmodeled MSV using radial basis function NNs, which are applied to identify unknown dynamics. In [21], an error transformation function is incorporated in the guidance part of the path following controller for an underactuated MSV. To overcome the saturation of the vehicle actuator, an auxiliary system is constructed by utilizing switching functions. In [22], an appointed-time PPC function is incorporated into trajectory tracking control of dynamic positioning vessels based on dynamics event-triggered mechanism. In [23], a state-feedback adjustable performance tracking control method is designed with all quantized states and control inputs. In [24], a dedicated robust adaptive NN predefined performance dynamic positioning scheme is developed for marine vehicles with model uncertainties, environmental disturbances, and input saturation. In [25], a continuous adaptive trajectory tracking control for uncertain MSV is investigated considering the singularity of control laws. in [26], a data-driven PPC scheme without prior model information is developed for surface vehicles via the reinforcement learning technique.

Notice that the above works pay more attention to the prescribed performance control of a single MSV. In contrast,

the prescribed performance coordination control of multiple MSVs is increasingly challenging due to limited communication ability and inter-individual connections [27]. Up to now, literature [20], [28], [29], [30], [31], [32], [33], [34], [35] report some prescribed performance formation control schemes for a swarm of MSVs. Based on the leader-following structure, [28] proposes a low-complexity PPC method with relaxed initial conditions for multiple marine vessels. In [29], a decentralized leader-following control strategy is proposed to achieve a collision-free formation of multiple vessels. In [30], a formation tracking algorithm based on the leader-following method is devised, which is capable not only of guaranteeing the predefined transient properties but also of achieving connectivity maintenance and collision avoidance. In [31], using only relative state signals, a robust leader-follower formation control scheme is derived for multiple MSVs with connectivity-maintaining and collision-avoiding abilities. In [33], a two-layer robust adaptive fault-tolerant formation controller is presented for marine vehicles under guaranteed performance. In [32], a prescribed performance containment control method is studied for multiple surface vehicles using a fuzzy-adaptive output-feedback scheme. In [20], a neural-learning-based control method with guaranteed transient performances is presented for marine vehicles without prior model dynamics. Utilizing dynamic surface control techniques, [34] develops a platoon formation PPC scheme for multiple marine vessels, which is capable of achieving the platoon proceeds along a given trajectory. In [35], a performance-guaranteed formation controller is presented by using the cooperative deterministic learning technique. It is seen that prescribed performance coordination controllers in [20], [28], [29], [33], [34], and [35] are designed for full-actuated MSVs. Due to no independent sway actuator, it is increasingly challenging to achieve the performance-prescribed coordination for underactuated MSVs.

From the above observations, the existing PPC methods are developed for a single MSV or a specific collective scenario, thus lacking application flexibility. Although these PPC methods can characterize the transient and state-steady performance of tracking error, there still exists an obvious transient overshoot to be addressed via a tedious tuning procedure. For marine vehicles, the thruster fault is usually unavoidable due to device aging and environmental factors [36], [37]. Owing to the inflexibility of PPC boundaries, the fault-affected tracking error may breach user-specified bounds. Besides, it is even more challenging for underactuated MSVs due to no sway actuator [30], [31], [32].

Motivated by above discussions, we aim to develop an echo state network-based (ESN-based) transient-reinforced tunnel coordinated control method of multiple underactuated MSVs. The main highlights are summarized below.

- In contrast to the existing PPC coordination methods designed for a specific collective scenario in [28], [29], [30], [31], [32], [33], [20], [34], and [35], the proposed transient-reinforced tunnel coordinated method is a general case of previous results and more suitable for practical applications, where a graph-based trajectory generator is designed to achieve various collaborative behaviors.
- In contrast to the PPC methods proposed in [18], [19], [20], [21], [22], [23], [24], [25], [26], [28], [29], [30], [31], [32], [33], [34], [35], and [38], the tunnel prescribed performance (TPP) functions for position and heading constraints of underactuated MSVs are developed to reinforce the overshoot and accuracy of coordination. Based on the TPP transformation, the tunnel guidance laws can overcome the obvious overshoot without tedious tuning procedures.
- In contrast to the NN, fuzzy approximation and observer techniques proposed in [20], [28], [29], [30], [31], [32], [33], [34], [35], and [39], the ESN-based neural estimators are derived to recover the total disturbance of the vehicle's kinetics under fully unknown actuator faults. Then, the tunnel performance of multi-MSV coordination can be guaranteed regardless of actuator faults using the ESN-based control method.

This paper is organized as below. Section II introduces preliminaries and problem formulation. Section III provides the controller design. Section IV proves the stability. Section V gives simulation results. Section VI concludes this paper.

II. Preliminaries and Problem Formulation

A. Preliminaries

1) Notations: Throughout this paper, $\Re^{m\times n}$ represents an $m \times n$-dimensional Euclidean space. diag$\{\cdots\}$ is a block-diagonal matrix. $\|\cdot\|$ denotes the Euclidean norm of a vector or matrix. sgn(x) represents a sign function with sgn$(x) = 1$ for $x > 0$, sgn$(x) = -1$ for $x < 0$, and sgn$(x) = 0$ for $x = 0$.

2) Graph theory: Consider a networked system with N follower MSVs and M virtual leaders. A graph $\mathcal{G}$ is defined as $\mathcal{G} = \{\mathcal{V}, \mathcal{E}\}$, where $\mathcal{V}$ is a node set with $\mathcal{V} = \{\mathcal{V}^F, \mathcal{V}^L\}$ being the sets of MSVs and the virtual leader, and $\mathcal{E}$ is an edge set with $\mathcal{E} = \{(i, j) \in \mathcal{V} \times \mathcal{V}\}$. Define the neighborhood set $\mathcal{N}_i$ of the i-th MSV as $\mathcal{N}_i = \{\mathcal{N}_i^F, \mathcal{N}_i^L\}$, where $\mathcal{N}_i^F = \{j \in \mathcal{V}_i^F | (i, j) \in \mathcal{E}\}$ and $\mathcal{N}_i^L = \{j \in \mathcal{V}_i^L | (i, j) \in \mathcal{E}\}$.

B. Problem Formulation

Consider a networked multi-MSV system in Fig. 1. Two reference frames, a body reference frame {B} and an NED reference frame {E}, are usually used to describe the vehicle motion. According to [40], the motion dynamics of the $i$the MSV is described as

$$\begin{cases} \dot{\boldsymbol{\eta}}_i = \boldsymbol{R}(\psi_i)\boldsymbol{v}_i \\ \boldsymbol{M}_i\dot{\boldsymbol{v}}_i + \boldsymbol{C}_i\boldsymbol{v}_i + \boldsymbol{D}_i\boldsymbol{v}_i + \boldsymbol{g}_i = \boldsymbol{\tau}_i + \boldsymbol{\tau}_{id} \end{cases} \tag{1}$$

where $i = 1, \cdots, N$; $\boldsymbol{\eta}_i = [\boldsymbol{p}_i^T, \psi_i]^T \in \Re^3$ with $\boldsymbol{p}_i^T = [x_i, y_i]^T \in \Re^2$ being a position vector and ψ_i being a heading angle in $\{E\}$; $\boldsymbol{v}_i = [u_i, v_i, w_i]^T \in \Re^3$ denotes the surge, sway, and yaw velocity vector in $\{B\}$; $\boldsymbol{R}(\psi_i)$ is a rotation matrix satisfying $\boldsymbol{R}^{-1}(\psi_i) = \boldsymbol{R}^T(\psi_i)$ and $\dot{\boldsymbol{R}}(\psi_i) = w_i\boldsymbol{J}\boldsymbol{R}(\psi_i)$ with

$$\boldsymbol{R}_i = \begin{bmatrix} \cos\psi_i & -\sin\psi_i & 0 \\ \sin\psi_i & \cos\psi_i & 0 \\ 0 & 0 & 1 \end{bmatrix}, \quad \boldsymbol{J} = \begin{bmatrix} 0 & -1 & 0 \\ 1 & 0 & 0 \\ 0 & 0 & 0 \end{bmatrix};$$

$\boldsymbol{M}_i = \text{diag}\{m_{iu}, m_{iv}, m_{iw}\} \in \Re^{3\times3}$ is an inertial matrix; $\boldsymbol{C}_i = -\boldsymbol{C}_i^T \in \Re^{3\times3}$ is a Coriolis and centripetal matrix;

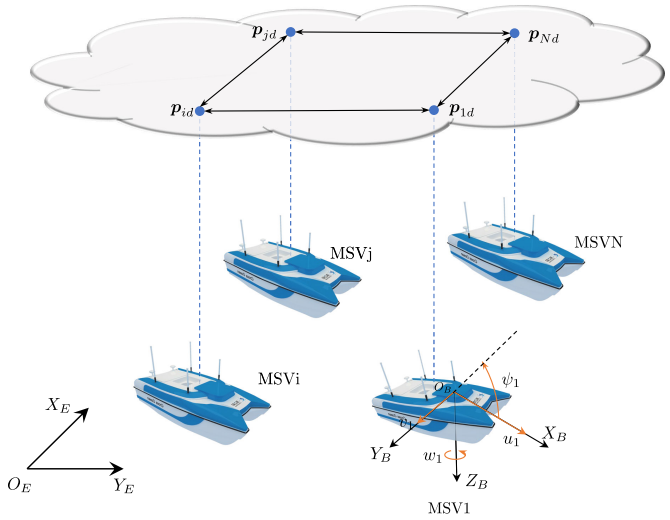

Fig. 1. The networked structure of underactuated MSVs.

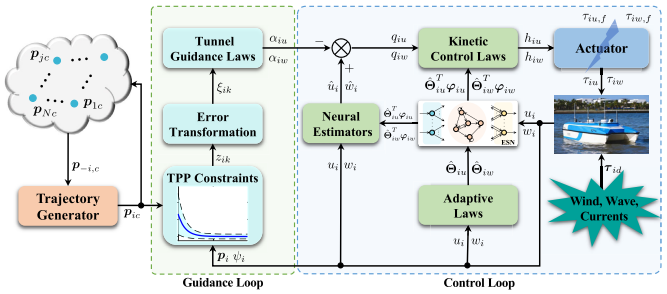

Fig. 2. The diagram of proposed ESN-based transient-reinforced tunnel coordinated control method.

$\boldsymbol{D}_i \in \Re^{3\times 3}$ is a hydrodynamic damping matrix; $\boldsymbol{g}_i \in \Re^3$ represents unmodelled hydrodynamics and modelling error; $\boldsymbol{\tau}_{id} \in \Re^3$ stands for bounded environmental disturbances caused by wind, wave, and current; $\boldsymbol{\tau}_i = [\tau_{iu}, 0, \tau_{iw}] \in \Re^3$ is the actual control vector with τ_{iu} being the surge force and τ_{iw} being the yaw moment. In a practical application, the thrusters of MSVs may suffer from faults expressed as

$$\tau_{ij} = \gamma_{ij}(t)h_{ij} + \tau_{ij,f}(t, t_1), \quad j = u, w \tag{2}$$

where $\gamma_{ij}(t) \in \Re$ is an actuator effectiveness; $\tau_{ik,f}(t) \in \Re$ denotes an additive fault segment; $h_{ij} \in \Re$ is the desired control input.

Assumption 1 ([41]): For MSVs, there exist positive constants $\underline{\gamma}_{ij} \in \Re$ and $\bar{\tau}_{ij}^f \in \Re$ such that $\underline{\gamma}_{ij} \le \gamma_{ij}(t) \le 1$ and $|\tau_{ij,f}(t)| \le \bar{\tau}_{ij,f}$ for $j = u, w$.

1) Control objective: This paper aims to develop an ESN-based transient-reinforced tunnel coordinated control method for a group of underactuated MSVs subject to actuator faults such that: 1) each MSV can follow the reference trajectory satisfying $\|\boldsymbol{p}_i - \boldsymbol{p}_{ic}\| < \epsilon_{ip} \in \Re^+$ and $|\psi_i - \psi_{id}| < \epsilon_{i\psi} \in \Re^+$, where $\boldsymbol{p}_{ic}$ and ψ_{id} will be defined in the forthcoming section; 2) the position and heading tracking errors evolve within TPP constraint spaces regardless of actuator faults; 3) all errors of closed-loop system are ultimately bounded.

III. Controller Design

In this section, an ESN-based transient-reinforced tunnel coordinated control method is developed for a group of underactuated MSVs in the presence of internal uncertainties, external disturbances, and actuator faults. The diagram block of proposed method is shown in Fig. 2.

A. Trajectory Generator Design

Looking back at the existing performance-prescribed control schemes proposed in [8], [28], [29], [31], and [35], these coordinated controllers are designed for a specific mission scenario. Once the coordination scenario changes, experts or engineers have to redevelop new control laws for accomplishing the control objective. Thus, it is necessary to develop a coordinated method capable of implementing various mission patterns. Inspired by this limitation, we design a graph-based trajectory generator for a specific coordination scenario as follows

$$\begin{cases} \dot{\boldsymbol{p}}_{ic} &= \boldsymbol{q}_{ic} \\ \dot{\boldsymbol{q}}_{ic} &= \hbar_i\left(t, \boldsymbol{p}_{ic}, \boldsymbol{q}_{ic}, \boldsymbol{p}_{-i,c}, \boldsymbol{q}_{-i,c}\right) \end{cases} \tag{3}$$

where $\boldsymbol{p}_{ic} = [x_{ic}, y_{ic}]^T \in \Re^2$ and $\boldsymbol{q}_{ic} = [q_{ixc}, q_{iyc}]^T \in \Re^2$ are the desired reference signals; The coordination function $\hbar_i(\cdot) \in \Re^2$ is known, bounded, and continuously differential; $\boldsymbol{p}_{-i,c} \in \Re^2$ and $\boldsymbol{q}_{-i,c} \in \Re^2$ denote state sets of neighboring nodes defined as $\boldsymbol{p}_{-i,c} = \{\boldsymbol{p}_{jc}\}_{j\in\mathcal{N}_i^F \bigcup \mathcal{N}_i^L}$ and $\boldsymbol{q}_{-i,c} = \{\boldsymbol{q}_{jc}\}_{j\in\mathcal{N}_i^F \bigcup \mathcal{N}_i^L}$.

Remark 1: Herein, the proposed coordinated control method with the trajectory generator (3) belongs to the decentralized architecture. Compared with the distributed control, decentralized control has a simpler architecture and lower calculation cost [27]. Moreover, the decentralized control architecture takes the advantage of failure tolerance, modularity, and scalability. Because of these advantages, the decentralized control architecture has been widely applied in the formation control, target tracking, and platoon control of marine vehicles, see references [34], [42], [43], [44], and [45].

B. Guidance Law Design for Kinematics

To track the reference information $\boldsymbol{p}_{ic}$ broadcasted from (3), a tracking error is defined as $\boldsymbol{p}_{ie} = [x_{ie}, y_{ie}] = \boldsymbol{p}_{ic} - \boldsymbol{p}_i$. Then, the relative distance E_i and the relative heading ψ_{ie} are derived as follows

$$E_i = \sqrt{x_{ie}^2 + y_{ie}^2}, \quad \psi_{ie} = \psi_{id} - \psi_i \tag{4}$$

with $\psi_{id} \in (-\pi, \pi]$ being a desired heading angle with respect to $\boldsymbol{p}_{ic}$ defined below [46]

$$\psi_{id} = \text{atan2}(y_{ie}, x_{ie}) \tag{5}$$

where $\text{atan2}(\cdot,\cdot)$ is an inverse tangent function. Notice that ψ_{id} is not well defined due to no definition of $\text{atan2}(\cdot,\cdot)$ at $(0,0)$, i.e. ψ_{id} is not defined when $E_i = 0$. In the subsequent design, we will design the guidance law to force the relative distance within the performance constraints. Thus, the no definition of $\psi_{id}|_{(0,0)}$ can be avoided for $E_i > 0, \forall t \ge 0$.

In a practical application, most of marine vehicles are typically underactuated systems, i.e. there are only thrusters in the surge and yaw directions. The underactuation property makes it more challenging to derive the guidance laws for errors E_i and ψ_{ie} [47], [48]. In addition, the standard PPC proposed in [23], [34], and [49] have exponential-type performance bounds distributed on both sides of the origin, which still lead to the obvious overshoots without tedious tuning procedures.

To reinforce the position and heading coordinated performance, the TPP constraints are established to limit errors

$$0 < z_{iE} < z_{iE}^r \tag{6}$$

$$-z_{i\psi}^l < z_{i\psi} < z_{i\psi}^r \tag{7}$$

where $z_{iE} = E_i$ and $z_{i\psi} = \psi_{ie}$

$$\begin{cases} z_{iE}^r &= [\delta_{iE}^r + \mathrm{sgn}(z_{iE,0})]\rho_{iE}(t) - \rho_{iE,\infty}\,\mathrm{sgn}(z_{iE,0}) \\ z_{i\psi}^r &= [\delta_{i\psi}^r + \mathrm{sgn}(z_{i\psi,0})]\rho_{i\psi}(t) - \rho_{i\psi,\infty}\,\mathrm{sgn}(z_{i\psi,0}) \\ z_{i\psi}^l &= [\delta_{i\psi}^l - \mathrm{sgn}(z_{i\psi,0})]\rho_{i\psi}(t) + \rho_{i\psi,\infty}\,\mathrm{sgn}(z_{i\psi,0}) \end{cases} \tag{8}$$

where $0 \le \delta_{ik}^r, \delta_{ik}^l \le 1$; $\rho_{ik}(t)$ is a prescribed potential function defined as $\rho_{ik}(t) = (\rho_{ik,0} - \rho_{ik,\infty})e^{-\mu_{ik}t} + \rho_{ik,\infty}$ with $\rho_{ik,0} = z_{ik}(0)$, $\rho_{ik,\infty} = \lim_{t\to\infty}\rho_{ik}(t)$, $\rho_{ik,0} > \rho_{ik,\infty} > 0$, and $\mu_{ik} \in \Re^+$ for $k = E, \psi$.

Based on the PPC methodology, z_{ik} need to be equivalently transformed as an unconstrained variable ξ_{ik} by an error transformation function (ETF) formulated as [50]

$$z_{ik} = \frac{z_{ik}^r + z_{ik}^l}{2}\Upsilon(\xi_{ik}) + \frac{z_{ik}^r - z_{ik}^l}{2}, \quad k = E, \psi \tag{9}$$

where $\Upsilon(\xi_{ik})$ is a smooth and strictly increasing function satisfying the following properties

$$\begin{cases} \lim\limits_{\xi_{ik}\to\infty}\Upsilon(\xi_{ik}) = 1 \\ \lim\limits_{\xi_{ik}\to-\infty}\Upsilon(\xi_{ik}) = -1 \\ \Upsilon(0) = 0. \end{cases} \tag{10}$$

Considering the properties (10), $\Upsilon(\xi_{ik})$ can be selected as

$$\Upsilon(\xi_{ik}) = \frac{2}{\pi}\arctan(\xi_{ik}). \tag{11}$$

and the corresponding inverse function is deduced as

$$\xi_{ik} = \Upsilon^{-\mathrm{inv}}(z_{ik}, z_{ik}^r, z_{ik}^l) = \tan\left[\frac{\pi}{2}\Upsilon(\xi_{ik})\right]. \tag{12}$$

Along (11) and (12), it takes the derivative of ξ_{ik} that

$$\dot{\xi}_{ik} = \frac{\partial\xi_{ik}}{\partial\Upsilon(\xi_{ik})}\left[\frac{\partial\Upsilon(\xi_{ik})}{\partial z_{ik}}\dot{z}_{ik} + \frac{\partial\Upsilon(\xi_{ik})}{\partial z_{ik}^r}\dot{z}_{ik}^r + \frac{\partial\Upsilon(\xi_{ik})}{\partial z_{ik}^l}\dot{z}_{ik}^l\right] \tag{13}$$

where $\partial\xi_{ik}/\partial\Upsilon(\xi_{ik}) = \pi\sec^2[\pi\Upsilon(\xi_{ik})/2]/2$, $\partial\Upsilon(\xi_{ik})/\partial z_{ik} = 2/(z_{ik}^r + z_{ik}^l)$, $\partial\Upsilon(\xi_{ik})/\partial z_{ik}^r = -2(z_{ik} + z_{ik}^l)/(z_{ik}^r + z_{ik}^l)^2$, and $\partial\Upsilon(\xi_{ik})/\partial z_{ik}^l = -2(z_{ik} - z_{ik}^r)/(z_{ik}^r + z_{ik}^l)^2$.

For brevity of presentation, we rewrite $\mathcal{F}_{z_{ik}} = [\partial\xi_{ik}/\partial\Upsilon(\xi_{ik})][\partial\Upsilon(\xi_{ik})/\partial z_{ik}]$, $\mathcal{F}_{z_{ik}^r} = [\partial\xi_{ik}/\partial\Upsilon(\xi_{ik})][\partial\Upsilon(\xi_{ik})/\partial z_{ik}^r]$, and $\mathcal{F}_{z_{ik}^l} = [\partial\xi_{ik}/\partial\Upsilon(\xi_{ik})][\partial\Upsilon(\xi_{ik})/\partial z_{ik}^l]$. Then, the dynamics of ξ_{ik}, $k = E, \psi$ are further presented by

$$\begin{cases} \dot{\xi}_{iE} = & \mathcal{F}_{z_{iE}}\dot{z}_{iE} + \mathcal{F}_{z_{iE}^r}\dot{z}_{iE}^r \\ \dot{\xi}_{i\psi} = & \mathcal{F}_{z_{i\psi}}\dot{z}_{i\psi} + \mathcal{F}_{z_{i\psi}^r}\dot{z}_{i\psi}^r + \mathcal{F}_{z_{i\psi}^l}\dot{z}_{i\psi}^l. \end{cases} \tag{14}$$

Let $u_{ie} = u_i - \alpha_{iu}$ and $w_{ie} = w_i - \alpha_{iw}$ with α_{iu} and α_{iw} being the desired surge and yaw guidance laws, respectively. Thus, it substitutes u_{ie} and w_{ie} into (14) using $x_{ie} = E_i\cos\psi_{id}$ and $y_{ie} = E_i\sin\psi_{id}$ as below

$$\begin{cases} \dot{\xi}_{iE} = & \mathcal{F}_{z_{iE}}\Big[2u_i\sin^2(\frac{\psi_{ie}}{2}) - v_i\sin\psi_{ie} - \alpha_{iu} \\ & -u_{ie} + \dot{x}_{id}\cos(\psi_{id}) + \dot{y}_{id}\sin(\psi_{id})\Big] \\ & + \mathcal{F}_{z_{iE}^r}\dot{z}_{iE}^r \\ \dot{\xi}_{i\psi} = & \mathcal{F}_{z_{i\psi}}(-\alpha_{iw} - w_{ie} + \dot{\psi}_{id}) + \mathcal{F}_{z_{i\psi}^r}\dot{z}_{i\psi}^r \\ & + \mathcal{F}_{z_{i\psi}^l}\dot{z}_{i\psi}^l. \end{cases} \tag{15}$$

In the guidance loop, the desired tunnel guidance laws are developed to satisfy the TPP constraints (6)-(8) as follows

$$\begin{cases} \alpha_{iu} = & \dot{x}_{id}\cos\psi_{id} + \dot{y}_{id}\sin\psi_{id} - v_i\sin\psi_{ie} \\ & + 2u_i\sin^2(\frac{\psi_{ie}}{2}) + \frac{1}{\mathcal{F}_{z_{iE}}}k_{iE}\xi_{iE} \\ & + \frac{1}{\mathcal{F}_{z_{iE}}}\mathcal{F}_{z_{iE}^r}\dot{z}_{iE}^r \\ \alpha_{iw} = & \dot{\psi}_{id} + \frac{1}{\mathcal{F}_{z_{i\psi}}}k_{i\psi}\xi_{i\psi} + \frac{1}{\mathcal{F}_{z_{i\psi}}}\mathcal{F}_{z_{i\psi}^r}\dot{z}_{i\psi}^r \\ & + \frac{1}{\mathcal{F}_{z_{i\psi}}}\mathcal{F}_{z_{i\psi}^l}\dot{z}_{i\psi}^l \end{cases} \tag{16}$$

where k_{iE} and $k_{i\psi}$ are positive constants.

Substituting (16) into (15), the dynamics of the kinematic subsystem are yielded as

$$\begin{cases} \dot{\xi}_{iE} &= -k_{iE}\xi_{iE} - \mathcal{F}_{z_{iE}}u_{ie} \\ \dot{\xi}_{i\psi} &= -k_{i\psi}\xi_{i\psi} - \mathcal{F}_{z_{i\psi}}w_{ie}. \end{cases} \tag{17}$$

C. Control Law Design for Kinetics

Next, rewrite the kinetic model of MSVs as below

$$\dot{\boldsymbol{v}}_i = \boldsymbol{f}_i(\boldsymbol{v}_i, t) + \boldsymbol{M}_i^{-1}\boldsymbol{\tau}_i \tag{18}$$

where $\boldsymbol{f}_i(\boldsymbol{v}_i, t) = [f_{iu}(\cdot), f_{iv}(\cdot), f_{iw}(\cdot)]^T = \boldsymbol{M}_i^{-1}(-\boldsymbol{C}_i\boldsymbol{v}_i - \boldsymbol{D}_i\boldsymbol{v}_i - \boldsymbol{g}_i + \boldsymbol{\tau}_{id})$ denotes the unknown kinetic function consisting of internal uncertainties and external disturbances.

For underactuated MSVs without the sway actuator, the surge and yaw dynamics are only considered herein

$$\begin{cases} \dot{u}_i &= F_{iu}(\cdot) + \frac{1}{m_{iu}}h_{iu} \\ \dot{w}_i &= F_{iw}(\cdot) + \frac{1}{m_{iw}}h_{iw} \end{cases} \tag{19}$$

where $F_{iu}(\cdot) = f_{iu}(\cdot) + (\gamma_{iu} - 1)h_{iu} + \tau_{iu,f}$ and $F_{iw}(\cdot) = f_{iw}(\cdot) + (\gamma_{iw} - 1)h_{iw} + \tau_{iw,f}$.

The NN approximation is an effective tool to identify the unknown time-invariant functions [51], [52], [53]. Herein,

ESNs are employed to recover the unknown terms $F_{iu}(\cdot)$ and $F_{iw}(\cdot)$

$$\begin{cases} F_{iu}(\cdot) &= \boldsymbol{\Theta}_{iu}^T \boldsymbol{\varphi}_{iu} + \epsilon_{iu} \\ F_{iw}(\cdot) &= \boldsymbol{\Theta}_{iw}^T \boldsymbol{\varphi}_{iw} + \epsilon_{iw} \end{cases} \tag{20}$$

where $\boldsymbol{\Theta}_{iu} \in \Re^m$ and $\boldsymbol{\Theta}_{iw} \in \Re^m$ are the output weight vectors of ESNs with $\|\boldsymbol{\Theta}_{iu}\| \le \bar{\Theta}_{iu} \in \Re^+$ and $\|\boldsymbol{\Theta}_{iw}\| \le \bar{\Theta}_{iw} \in \Re^+$; $\boldsymbol{\varphi}_{iu} \in \Re^m$ and $\boldsymbol{\varphi}_{iw} \in \Re^m$ are m-dimensional reservoir state vectors; ϵ_{iu} and ϵ_{iw} stand for approximation errors satisfying $|\epsilon_{iu}| \le \bar{\epsilon}_{iu} \in \Re^+$ and $|\epsilon_{iw}| \le \bar{\epsilon}_{iw} \in \Re^+$, respectively. Utilizing the exponential smoothing property of recurrent NN, the dynamics of $\boldsymbol{\varphi}_{iu}$ and $\boldsymbol{\varphi}_{iw}$ are updated by

$$\begin{cases} \dot{\boldsymbol{\varphi}}_{iu} = \dfrac{1}{T_{iu}}[-b_{iu}\boldsymbol{\varphi}_{iu} + \boldsymbol{\sigma}_{iu}(\boldsymbol{\Theta}_{iu}^{\boldsymbol{\chi}}\boldsymbol{\chi}_{iu} + \boldsymbol{\Theta}_{iu}^{\boldsymbol{\varphi}}\boldsymbol{\varphi}_{iu})] \\ \dot{\boldsymbol{\varphi}}_{iw} = \dfrac{1}{T_{iw}}[-b_{iw}\boldsymbol{\varphi}_{iw} + \boldsymbol{\sigma}_{iw}(\boldsymbol{\Theta}_{iw}^{\boldsymbol{\chi}}\boldsymbol{\chi}_{iw} + \boldsymbol{\Theta}_{iw}^{\boldsymbol{\varphi}}\boldsymbol{\varphi}_{iw})] \end{cases} \tag{21}$$

where $T_{iu} \in \Re^+$ and $T_{iw} \in \Re^+$ are time constants; $b_{iu} \in \Re^+$ and $b_{iw} \in \Re^+$ represent leaking rates; $\boldsymbol{\sigma}_{iu}(\cdot) \in \Re^m$ and $\boldsymbol{\sigma}_{iw}(\cdot) \in \Re^m$ are activation functions; $\boldsymbol{\chi}_{iu} = [u_i(t), u_i(t-t_d), h_{iu}(t)]^T$ and $\boldsymbol{\chi}_{iw} = [w_i(t), w_i(t-t_d), h_{iw}(t)]^T$ are the input vectors of ESNs with the sampling interval $t_d \in \Re^+$; $\boldsymbol{\Theta}_{iu}^{\boldsymbol{\chi}} \in \Re^{m\times 3}$ and $\boldsymbol{\Theta}_{iw}^{\boldsymbol{\chi}} \in \Re^{m\times 3}$, $\boldsymbol{\Theta}_{iu}^{\boldsymbol{\varphi}} \in \Re^{m\times m}$, and $\boldsymbol{\Theta}_{iw}^{\boldsymbol{\varphi}} \in \Re^{m\times m}$ denote the input and reservoir weights.

To identify the unknown components of dynamics (19), the ESN-based neural estimators are constructed as follows

$$\begin{cases} \dot{\hat{u}}_i &= -(\varsigma_{iu} + k_{iu}^o)\tilde{u}_i + \hat{\boldsymbol{\Theta}}_{iu}^T\boldsymbol{\varphi}_{iu} + \dfrac{1}{m_{iu}}h_{iu} \\ \dot{\hat{w}}_i &= -(\varsigma_{iw} + k_{iw}^o)\tilde{w}_i + \hat{\boldsymbol{\Theta}}_{iw}^T\boldsymbol{\varphi}_{iw} + \dfrac{1}{m_{iw}}h_{iw} \end{cases} \tag{22}$$

where $\tilde{u}_i = \hat{u}_i - u_i$ and $\tilde{w}_i = \hat{w}_i - w_i$; $\hat{u}_i$, $\hat{w}_i$, $\hat{\boldsymbol{\Theta}}_{iu}$, and $\hat{\boldsymbol{\Theta}}_{iw}$ are the estimation values of u_i, w_i, $\boldsymbol{\Theta}_{iu}$, and $\boldsymbol{\Theta}_{iw}$, respectively; $\varsigma_{iu} \in \Re^+$, $\varsigma_{iw} \in \Re^+$, $k_{iu}^o \in \Re^+$, and $k_{iw}^o \in \Re^+$ denote the estimator gains. $\hat{\boldsymbol{\Theta}}_{iu}$, and $\hat{\boldsymbol{\Theta}}_{iw}$ are updated by the adaptive law

$$\begin{cases} \dot{\hat{\boldsymbol{\Theta}}}_{iu} &= -\Gamma_{iu}(\boldsymbol{\varphi}_{iu}\tilde{u}_i + k_{iu}^{\boldsymbol{\Theta}}\hat{\boldsymbol{\Theta}}_{iu}) \\ \dot{\hat{\boldsymbol{\Theta}}}_{iw} &= -\Gamma_{iw}(\boldsymbol{\varphi}_{iw}\tilde{w}_i + k_{iw}^{\boldsymbol{\Theta}}\hat{\boldsymbol{\Theta}}_{iw}) \end{cases} \tag{23}$$

where $k_{iu}^{\boldsymbol{\Theta}} \in \Re$, $k_{iw}^{\boldsymbol{\Theta}} \in \Re$, $\Gamma_{iu} \in \Re$, and $\Gamma_{iw} \in \Re$ are positive tuning coefficients.

Define $\tilde{\boldsymbol{\Theta}}_{iu} = \hat{\boldsymbol{\Theta}}_{iu} - \boldsymbol{\Theta}_{iu}$ and $\tilde{\boldsymbol{\Theta}}_{iw} = \hat{\boldsymbol{\Theta}}_{iw} - \boldsymbol{\Theta}_{iw}$, and take their derivatives together with $\tilde{u}_i$ and $\tilde{w}_i$ as

$$\begin{cases} \dot{\tilde{u}}_i = -(\varsigma_{iu} + k_{iu}^o)\tilde{u}_i + \tilde{\boldsymbol{\Theta}}_{iu}^T\boldsymbol{\varphi}_{iu} - \epsilon_{iu} \\ \dot{\tilde{\boldsymbol{\Theta}}}_{iu} = -\Gamma_{iu}(\boldsymbol{\varphi}_{iu}\tilde{u}_i + k_{iu}^{\boldsymbol{\Theta}}\hat{\boldsymbol{\Theta}}_{iu}) \\ \dot{\tilde{w}}_i = -(\varsigma_{iw} + k_{iw}^o)\tilde{w}_i + \tilde{\boldsymbol{\Theta}}_{iw}^T\boldsymbol{\varphi}_{iw} - \epsilon_{iw} \\ \dot{\tilde{\boldsymbol{\Theta}}}_{iw} = -\Gamma_{iw}(\boldsymbol{\varphi}_{iw}\tilde{w}_i + k_{iw}^{\boldsymbol{\Theta}}\hat{\boldsymbol{\Theta}}_{iw}). \end{cases} \tag{24}$$

Let $q_{iu} = \hat{u}_i - \alpha_{iu}$ and $q_{iw} = \hat{w}_i - \alpha_{iw}$. Then, the derivatives of q_{iu} and q_{iw} using (22) are presented as

$$\begin{cases} \dot{q}_{iu} &= -(\varsigma_{iu} + k_{iu}^o)\tilde{u}_i + \hat{\boldsymbol{\Theta}}_{iu}^T\boldsymbol{\varphi}_{iu} + \dfrac{h_{iu}}{m_{iu}} - \dot{\alpha}_{iu} \\ \dot{q}_{iw} &= -(\varsigma_{iw} + k_{iw}^o)\tilde{w}_i + \hat{\boldsymbol{\Theta}}_{iw}^T\boldsymbol{\varphi}_{iw} + \dfrac{h_{iw}}{m_{iw}} - \dot{\alpha}_{iw}. \end{cases} \tag{25}$$

To stabilize the dynamics in (25), the ESN-based surge and yaw control laws are designed as below

$$\begin{cases} h_{iu} = \ m_{iu}(-k_{iu}q_{iu} - \hat{\boldsymbol{\Theta}}_{iu}^T\boldsymbol{\varphi}_{iu} + \dot{\alpha}_{iu}) \\ h_{iw} = \ m_{iw}(-k_{iw}q_{iw} - \hat{\boldsymbol{\Theta}}_{iw}^T\boldsymbol{\varphi}_{iw} + \dot{\alpha}_{iw}) \end{cases} \tag{26}$$

where k_{iu} and k_{iw} are positive constants.

Combining (25) and (26), the control subsystem follows that

$$\begin{cases} \dot{q}_{iu} &= -k_{iu}q_{iu} - (\varsigma_{iu} + k_{iu}^o)\tilde{u}_i \\ \dot{q}_{iw} &= -k_{iw}q_{iw} - (\varsigma_{iw} + k_{iw}^o)\tilde{w}_i. \end{cases} \tag{27}$$

IV. Main Results

The section analyzes the stability of the closed-loop transient-reinforced tunnel coordinated control system cascaded by the subsystems (17), (24), and (27). In the upcoming, the stability of subsystem (24) is shown by Lemme 1.

Lemma 1: The subsystem (24) regarded as a system with the states $\tilde{u}_i$, $\tilde{u}_i$, $\tilde{\boldsymbol{\Theta}}_{iu}$, and $\tilde{\boldsymbol{\Theta}}_{iw}$ and the inputs ϵ_{iu}, ϵ_{iw}, $\boldsymbol{\Theta}_{iu}$, and $\boldsymbol{\Theta}_{iw}$ is ISS.

Proof: Construct a Lyapunov function candidate V_{io} for (24) as follows

$$V_{io} = \frac{1}{2}\sum_{i=1}^{N}\left(\tilde{u}_i^2 + \tilde{w}_i^2 + \frac{1}{\Gamma_{iu}}\tilde{\boldsymbol{\Theta}}_{iu}^T\tilde{\boldsymbol{\Theta}}_{iu} + \frac{1}{\Gamma_{iw}}\tilde{\boldsymbol{\Theta}}_{iw}^T\tilde{\boldsymbol{\Theta}}_{iw}\right) \tag{28}$$

and take its derivative as

$$\begin{aligned} \dot{V}_{io} = \sum_{i=1}^{N}\Big[& -\tilde{u}_i[(\varsigma_{iu} + k_{iu}^o)\tilde{u}_i - \tilde{\boldsymbol{\Theta}}_{iu}^T\boldsymbol{\varphi}_{iu} + \epsilon_{iu}] \\ & - \tilde{w}_i[(\varsigma_{iw} + k_{iw}^o)\tilde{w}_i - \tilde{\boldsymbol{\Theta}}_{iw}^T\boldsymbol{\varphi}_{iw} + \epsilon_{iw}] \\ & - \tilde{\boldsymbol{\Theta}}_{iu}^T(\boldsymbol{\varphi}_{iu}\tilde{u}_i + k_{iu}^{\boldsymbol{\Theta}}\hat{\boldsymbol{\Theta}}_{iu}) \\ & - \tilde{\boldsymbol{\Theta}}_{iu}^T(\boldsymbol{\varphi}_{iu}\tilde{u}_i + k_{iu}^{\boldsymbol{\Theta}}\hat{\boldsymbol{\Theta}}_{iu})\Big] \\ = \sum_{i=1}^{N}\Big[& -(\varsigma_{iu} + k_{iu}^o)\tilde{u}_i^2 - (\varsigma_{iw} + k_{iw}^o)\tilde{w}_i^2 - \tilde{u}_i\epsilon_{iu} \\ & - \tilde{w}_i\epsilon_{iw} - k_{iu}^{\boldsymbol{\Theta}}\tilde{\boldsymbol{\Theta}}_{iu}^T\hat{\boldsymbol{\Theta}}_{iu} - k_{iw}^{\boldsymbol{\Theta}}\tilde{\boldsymbol{\Theta}}_{iw}^T\hat{\boldsymbol{\Theta}}_{iw}\Big]. \end{aligned} \tag{29}$$

Since $-k_{iu}^{\boldsymbol{\Theta}}\tilde{\boldsymbol{\Theta}}_{iu}^T\hat{\boldsymbol{\Theta}}_{iu} = -k_{iu}^{\boldsymbol{\Theta}}\tilde{\boldsymbol{\Theta}}_{iu}^T(\tilde{\boldsymbol{\Theta}}_{iu} + \boldsymbol{\Theta}_{iu}) \le -k_{iu}^{\boldsymbol{\Theta}}\|\tilde{\boldsymbol{\Theta}}_{iu}\|^2 + k_{iu}^{\boldsymbol{\Theta}}\|\tilde{\boldsymbol{\Theta}}_{iu}\|\|\boldsymbol{\Theta}_{iu}\|$, $-k_{iw}^{\boldsymbol{\Theta}}\tilde{\boldsymbol{\Theta}}_{iw}^T\hat{\boldsymbol{\Theta}}_{iw} = -k_{iw}^{\boldsymbol{\Theta}}\tilde{\boldsymbol{\Theta}}_{iw}^T(\tilde{\boldsymbol{\Theta}}_{iw} + \boldsymbol{\Theta}_{iw}) \le -k_{iw}^{\boldsymbol{\Theta}}\|\tilde{\boldsymbol{\Theta}}_{iw}\|^2 + k_{iw}^{\boldsymbol{\Theta}}\|\|\tilde{\boldsymbol{\Theta}}_{iw}\|\|\boldsymbol{\Theta}_{iw}\|$, $\dot{V}_{io}$ is yielded as

$$\begin{aligned} \dot{V}_{io} \le \sum_{i=1}^{N}\Big[& -(\varsigma_{iu} + k_{iu}^o)\tilde{u}_i^2 - (\varsigma_{iw} + k_{iw}^o)\tilde{w}_i^2 + |\tilde{u}_i||\epsilon_{iu}| \\ & + |\tilde{w}_i||\epsilon_{iw}| - k_{iu}^{\boldsymbol{\Theta}}\|\tilde{\boldsymbol{\Theta}}_{iu}\|^2 - k_{iw}^{\boldsymbol{\Theta}}\|\tilde{\boldsymbol{\Theta}}_{iw}\|^2 \\ & + k_{iu}^{\boldsymbol{\Theta}}\|\tilde{\boldsymbol{\Theta}}_{iu}\|\|\boldsymbol{\Theta}_{iu}\| + k_{iw}^{\boldsymbol{\Theta}}\|\|\tilde{\boldsymbol{\Theta}}_{iw}\|\|\boldsymbol{\Theta}_{iw}\|\Big] \\ = \sum_{i=1}^{N}\Big[& -\boldsymbol{\Xi}_{io}^T\boldsymbol{A}_{io}\boldsymbol{\Xi}_{io} + \boldsymbol{\Xi}_{io}^T\boldsymbol{B}_{io}\Big] \end{aligned} \tag{30}$$

where $\boldsymbol{\Xi}_{io} = [|\tilde{u}_i|, |\tilde{w}_i|, \|\tilde{\boldsymbol{\Theta}}_{iu}\|, \|\tilde{\boldsymbol{\Theta}}_{iw}\|]^T$, $\boldsymbol{B}_{io} = [|\epsilon_{iu}|, |\epsilon_{iw}|, \|\boldsymbol{\Theta}_{iu}\|, \|\boldsymbol{\Theta}_{iw}\|]^T$, and

$$\boldsymbol{A}_{io} = \begin{bmatrix} \varsigma_{iu} + k_{iu}^o & 0 & 0 & 0 \\ 0 & \varsigma_{iw} + k_{iw}^o & 0 & 0 \\ 0 & 0 & k_{iu}^{\boldsymbol{\Theta}} & 0 \\ 0 & 0 & 0 & k_{iw}^{\boldsymbol{\Theta}} \end{bmatrix}.$$

Furthermore, (30) is put into

$$\dot{V}_{io} \leq \sum_{i=1}^{N}\Big[-\lambda_{\min}(\boldsymbol{A}_{io})\|\boldsymbol{\Xi}_{io}\|^2+\|\boldsymbol{B}_{io}\|\|\boldsymbol{\Xi}_{io}\|\Big] \tag{31}$$

where $\lambda_{\min}(\cdot)$ is the minimum eigenvalue of a matrix.

When $\|\boldsymbol{\Xi}_{io}\| \geq \|\boldsymbol{B}_{io}\|/\varrho_{io}\lambda_{\min}(\boldsymbol{A}_{io})$ with $0<\varrho_{io}<1$, one has

$$\dot{V}_{io} \leq \sum_{i=1}^{N}\Big[-\lambda_{\min}(\boldsymbol{A}_{io})(1-\varrho_{io})\|\boldsymbol{\Xi}_{io}\|^2\Big]. \tag{32}$$

Due to the boundedness of ϵ_{iu}, ϵ_{iw}, $\boldsymbol{\Theta}_{iu}$, and $\boldsymbol{\Theta}_{iw}$, the vector $\boldsymbol{B}_{io}$ is bounded. Consequently, it is concluded that estimator subsystem (24) is ISS, and

$$\|\boldsymbol{\Xi}_{io}(t)\| \leq \max\left\{e^{-\lambda_{\min}(\boldsymbol{A}_{io})(1-\varrho_{io})(t-t_0)}, \frac{\|\boldsymbol{B}_{io}\|}{\varrho_{io}\lambda_{\min}(\boldsymbol{A}_{io})}\right\} \tag{33}$$

for $t \geq t_0$. ■

Next, the stability of the control subsystem (27) is stated via the following lemma.

Lemma 2: The subsystem (27) regarded as a system with the states q_{iu} and q_{iw} and the inputs $\tilde{u}_i$ and $\tilde{w}_i$ is ISS.

Proof: Consider a Lyapunov function candidate as

$$V_{iq} = \frac{1}{2}\sum_{i=1}^{N}\Big(q_{iu}^2+q_{iw}^2\Big). \tag{34}$$

Along (27), it differentiates V_{iq} as

$$\begin{aligned}\dot{V}_{iq} &= \sum_{i=1}^{N}\Big[-k_{iu}q_{iu}^2-(\varsigma_{iu}+k_{iu}^o)q_{iu}\tilde{u}_i \\ &\qquad -k_{iw}q_{iw}^2-(\varsigma_{iw}+k_{iw}^o)q_{iw}\tilde{w}_i\Big] \\ &\leq \sum_{i=1}^{N}\Big[-k_{iu}q_{iu}^2+(\varsigma_{iu}+k_{iu}^o)|q_{iu}||\tilde{u}_i| \\ &\qquad -k_{iw}q_{iw}^2+(\varsigma_{iw}+k_{iw}^o)|q_{iw}||\tilde{w}_i|\Big]\end{aligned} \tag{35}$$

Let $\boldsymbol{\Xi}_{iq}=[|q_{iu}|,|q_{iw}|]^T$ and $\tilde{\boldsymbol{\vartheta}}_i=[|\tilde{u}_i|,|\tilde{w}_i|]^T$ and rewrite the derivative of V_{iq} as follows

$$\begin{aligned}\dot{V}_{iq} &= \sum_{i=1}^{N}\Big[-\boldsymbol{\Xi}_{iq}^T\boldsymbol{A}_{iq}\boldsymbol{\Xi}_{iq}+\boldsymbol{\Xi}_{iq}\boldsymbol{B}_{iq}\tilde{\boldsymbol{\vartheta}}_i\Big] \\ \boldsymbol{A}_{iq} &= \begin{bmatrix}k_{iu} & 0\\ 0 & k_{iw}\end{bmatrix},\ \boldsymbol{B}_{iq}=\begin{bmatrix}\varsigma_{iu}+k_{iu}^o & 0\\ 0 & \varsigma_{iw}+k_{iw}^o\end{bmatrix}.\end{aligned} \tag{36}$$

Then, we have

$$\dot{V}_{iq} \leq \sum_{i=1}^{N}\Big[-\lambda_{\min}(\boldsymbol{A}_{iq})\|\boldsymbol{\Xi}_{iq}\|^2+\|\boldsymbol{\Xi}_{iq}\|\|\boldsymbol{B}_{iq}\|\|\tilde{\boldsymbol{\vartheta}}_i\|\Big]. \tag{37}$$

When $\|\boldsymbol{\Xi}_{iq}\| \geq \|\boldsymbol{B}_{iq}\|\|\tilde{\boldsymbol{\vartheta}}_i\|/\varrho_{iq}\lambda_{\min}(\boldsymbol{A}_{iq})$ deduces

$$\dot{V}_{iq} \leq \sum_{i=1}^{N}\Big[-\lambda_{\min}(\boldsymbol{A}_{iq})(1-\varrho_{iq})\|\boldsymbol{\Xi}_{iq}\|^2\Big]. \tag{38}$$

with $0<\varrho_{io}<1$.

According to Lemma 1, it shows that the control subsystem (27) is ISS, and the ultimate bound is

$$\|\boldsymbol{\Xi}_{iq}(t)\| \leq \max\left\{e^{-\lambda_{\min}(\boldsymbol{A}_{iq})(1-\varrho_{iq})(t-t_0)}, \frac{\|\boldsymbol{B}_{iq}\|\|\tilde{\boldsymbol{\vartheta}}_i\|}{\varrho_{iq}\lambda_{\min}(\boldsymbol{A}_{iq})}\right\} \tag{39}$$

for $t \geq t_0$. Moreover, $u_{ie}=q_{iu}-\tilde{u}_i$ and $w_{ie}=q_{iw}-\tilde{w}_i$ can renders that errors u_{ie} and w_{ie} are bounded from Lemmas 1-2. ■

Then, the following lemma shows the stability of the guidance subsystem (17).

Lemma 3: The subsystem (17) regarded as a system with the states ξ_{iE} and $\xi_{i\psi}$ and the inputs u_{ie} and w_{ie} is ISS.

Proof: Consider a Lyapunov function candidate as

$$V_{i\xi} = \frac{1}{2}\sum_{i=1}^{N}\Big(\xi_{iE}^2+\xi_{i\psi}^2\Big) \tag{40}$$

and differentiate V_{i1} along the dynamics (17) as

$$\begin{aligned}\dot{V}_{i\xi} &= \sum_{i=1}^{N}\Big(-k_{iE}\xi_{iE}^2-k_{i\psi}\xi_{i\psi}^2 \\ &\qquad -\xi_{iE}\mathcal{F}_{z_{iE}}u_{ie}-\xi_{i\psi}\mathcal{F}_{z_{i\psi}}w_{ie}\Big) \\ &\leq \sum_{i=1}^{N}\Big(-k_{iE}\xi_{iE}^2-k_{i\psi}\xi_{i\psi}^2 \\ &\qquad +|\xi_{iE}||\mathcal{F}_{z_{iE}}u_{ie}|+|\xi_{i\psi}|\mathcal{F}_{z_{i\psi}}w_{ie}|\Big)\end{aligned} \tag{41}$$

Denote $\boldsymbol{\Xi}_{i\xi}=[|\xi_{iE}|,|\xi_{i\psi}|]^T$ and $\boldsymbol{\vartheta}_{ie}=[|u_{ie}|,|w_{ie}|]^T$. Then, it results to

$$\begin{aligned}\dot{V}_{i\xi} &\leq \sum_{i=1}^{N}\Big(-\boldsymbol{\Xi}_{i\xi}^T\boldsymbol{A}_{i\xi}\boldsymbol{\Xi}_{i\xi}+\boldsymbol{\Xi}_{i\xi}^T\boldsymbol{B}_{i\xi}\boldsymbol{\vartheta}_{ie}\Big) \\ &\leq \sum_{i=1}^{N}\Big[-\lambda_{\min}(\boldsymbol{A}_{i\xi})\|\boldsymbol{\Xi}_{i\xi}\|^2+\|\boldsymbol{\Xi}_{i\xi}\|\|\boldsymbol{B}_{i\xi}\|\|\boldsymbol{\vartheta}_{ie}\|\Big].\end{aligned} \tag{42}$$

where

$$\boldsymbol{A}_{i\xi}=\begin{bmatrix}k_{iE} & 0\\ 0 & k_{iE}\end{bmatrix},\ \boldsymbol{B}_{i\xi}=\begin{bmatrix}\mathcal{F}_{z_{iE}} & 0\\ 0 & \mathcal{F}_{z_{i\psi}}\end{bmatrix}.$$

For $\|\boldsymbol{\Xi}_{i\xi}\| \geq \|\boldsymbol{B}_{i\xi}\|\|\boldsymbol{\vartheta}_{ie}\|/\varrho_{i\xi}\lambda_{\min}(\boldsymbol{A}_{i\xi})$, one obtains

$$\dot{V}_{i\xi} \leq \sum_{i=1}^{N}\Big[-\lambda_{\min}(\boldsymbol{A}_{i\xi})(1-\varrho_{i\xi})\|\boldsymbol{\Xi}_{i\xi}\|^2\Big] \tag{43}$$

with $0<\varrho_{i\xi}<1$. Therefore, the guidance subsystem (17) is ISS, and the ultimate bound for $t \geq t_0$ is expressed as

$$\|\boldsymbol{\Xi}_{i\xi}(t)\| \leq \max\left\{e^{-\lambda_{\min}(\boldsymbol{A}_{i\xi})(1-\varrho_{i\xi})(t-t_0)}, \frac{\|\boldsymbol{B}_{i\xi}\|\|\boldsymbol{\vartheta}_{ie}\|}{\varrho_{i\xi}\lambda_{\min}(\boldsymbol{A}_{i\xi})}\right\}. \tag{44}$$

■

Throughout the above analysis, the stabilities of all subsystems have been given by Lemmas 1-3. Subsequently, the

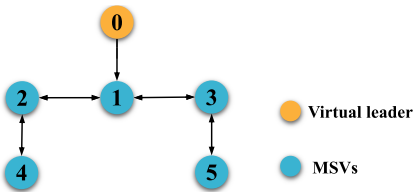

Fig. 3. The communication topology with one virtual leader.

stability of the presented closed-loop system is described by Theorem 1.

Theorem 1: For a fleet of underactuated MSVs (1) subject to actuator faults, the closed-loop ESN-based transient-reinforced tunnel coordinated system is ISS with the graph-based trajectory generator (3), the tunnel guidance law (16), the ESN-based neural estimator (22), the adaptive law (23), and the ESN-based control law (26). Besides, TPP constraints of position and heading errors do not be violated under actuator faults.

Proof: From Lemmas 1-3, the subsystems (24), (27), (17) are ISS. According to [54, Lemma 4.6], the system cascaded by the subsystems (24), (27), (17) is also ISS. By (33), it yields that the ultimate boundedness of $\|\boldsymbol{\Xi}_{io}(t)\|$ as $t \to \infty$

$$\|\boldsymbol{\Xi}_{io}(t)\|_{t\to\infty} \leq \frac{\sqrt{\bar{\epsilon}_{iu}^2 + \bar{\epsilon}_{iw}^2 + \bar{\Theta}_{iu}^2 + \bar{\Theta}_{iw}^2}}{\varrho_{io}\lambda_{\min}(\boldsymbol{A}_{io})}. \tag{45}$$

By the fact that $\|\tilde{\boldsymbol{\vartheta}}_i\| \leq \|\boldsymbol{E}_{io}\|$, one gets from (39) that

$$\|\boldsymbol{\Xi}_{iq}(t)\| \leq \frac{\|\boldsymbol{B}_{iq}\|\sqrt{\bar{\epsilon}_{iu}^2 + \bar{\epsilon}_{iw}^2 + \bar{\Theta}_{iu}^2 + \bar{\Theta}_{iw}^2}}{\varrho_{io}\varrho_{iq}\lambda_{\min}(\boldsymbol{A}_{iq})\lambda_{\min}(\boldsymbol{A}_{io})}. \tag{46}$$

From Lemmas 1-2, $\boldsymbol{\vartheta}_{ie}$ is bounded by $\bar{\vartheta}_i$. It follows from (44) that

$$\|\boldsymbol{\Xi}_{i\xi}(t)\|_{t\to\infty} \leq \frac{\|\boldsymbol{B}_{i\xi}\|}{\varrho_{i\xi}\lambda_{\min}(\boldsymbol{A}_{i\xi})}\bar{\vartheta}_i. \tag{47}$$

As a result, all error signals of the closed-loop system are uniformly ultimately bounded. The proof of Theorem 1 is completed. ■

V. Simulation Results

In this section, comparative simulation results are presented to validate the proposed ESN-based transient-reinforced tunnel coordinated control method. In this simulation, we consider a consensus-based coordination of five MSVs, labeled as MSV1, ..., MSV5. Fig. 3 gives a communication topology to describe the information exchanges.

To generate the consensus trajectories, the generator function $\boldsymbol{\hbar}_i$ by Fig. 3 is designed as

$$\boldsymbol{\hbar}_i = -l_i^2\Big[\sum_{j\in\mathcal{N}_i^F} a_{ij}(\boldsymbol{p}_{id} - \boldsymbol{p}_{jd} - \boldsymbol{\mathcal{P}}_{ijd}) - a_{i0}(\boldsymbol{p}_{id} - \boldsymbol{p}_{0d} - \boldsymbol{\mathcal{P}}_{i0d})\Big] - 2l_i\boldsymbol{q}_{id},\ i = 1,\ldots,5, \tag{48}$$

TABLE I
Parameters in the Simulation

Parameter	Value	Parameter	Value
$\rho_{iE,0}$	15	$\rho_{iE,\infty}$	0.5
$\rho_{i\psi,0}$	1.0	$\rho_{i\psi,\infty}$	0.1
μ_{iE}	0.1	$\mu_{i\psi}$	0.25
δ_{iE}, $\delta_{i\psi}$	0.6	$\delta_{i\psi}$	0.8
$\kappa_{iE,1}$	0.2	$\kappa_{iE,2}$	0.5
$\kappa_{i\psi,1}$	0.2	$\kappa_{i\psi,2}$	1.0
k_{iE}	0.1	$k_{i\psi}$	2.5
T_{iu}, T_{iw}	1.0	b_{iu}, b_{iw}	1.0
ς_{iu}, ς_{iw}	20	k_{iu}^o,k_{iw}^o	1.0
Γ_{iu}, Γ_{iw}	1000	k_{iu}^{Θ}, k_{iw}^{Θ}	0.0001
k_{iu}	10	k_{iw}	10

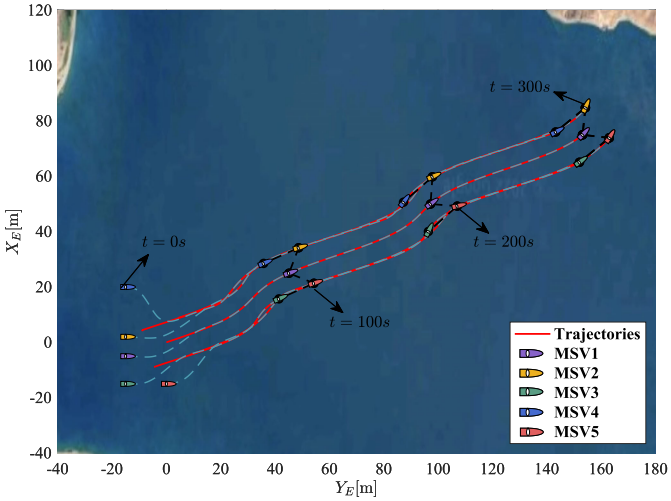

Fig. 4. The tracking trajectories of MSV1-MSV5 with the proposed method.

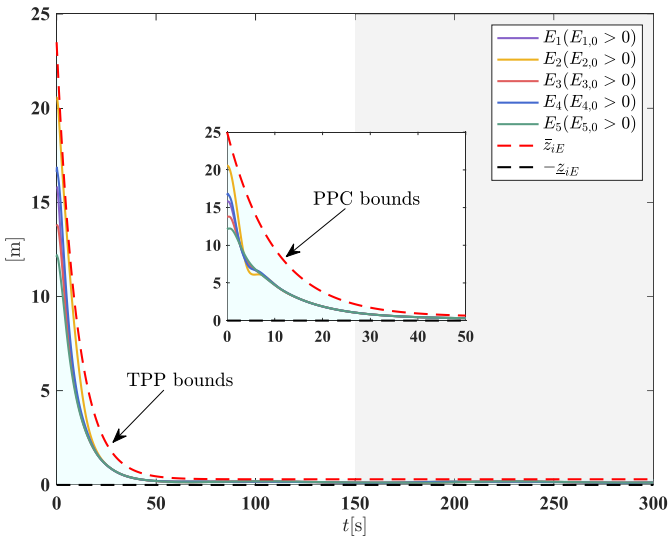

Fig. 5. The distance errors under proposed TPP constraint and standard PPC constraint proposed in [18].

where $\boldsymbol{p}_{1d}(0) = [0,0]^T$, $\boldsymbol{p}_{2d}(0) = [4.5,8.5]^T$, $\boldsymbol{p}_{3d}(0) = [9,-4.5]^T$, $\boldsymbol{p}_{4d}(0) = [-9,4.5]^T$, $\boldsymbol{p}_{5d}(0) = [-4.5,-9]^T$, and $\boldsymbol{q}_{id}(0) = [0,0]^T$; $\boldsymbol{\mathcal{P}}_{10d} = [0,0,0]^T$, $\boldsymbol{\mathcal{P}}_{20d} = \boldsymbol{R}_d[7,7,0]^T$, $\boldsymbol{\mathcal{P}}_{30d} = \boldsymbol{R}_d[7,-7,0]^T$, $\boldsymbol{\mathcal{P}}_{40d} = \boldsymbol{R}_d[-7,7,0]^T$, and $\boldsymbol{\mathcal{P}}_{50d} = \boldsymbol{R}_d[-7,-7,0]^T$ with $\boldsymbol{R}_d = \boldsymbol{R}(\psi_{0d})$ and $\psi_{0d} = \text{atan2}(\dot{y}_{0d}, \dot{x}_{0d})$. Initial status of five MSVs are set as $\boldsymbol{\eta}_1(0) = [-15,-5,0]^T$, $\boldsymbol{\eta}_2(0) = [-15,-2,0]^T$, $\boldsymbol{\eta}_3(0) = [0,-15,0]^T$,

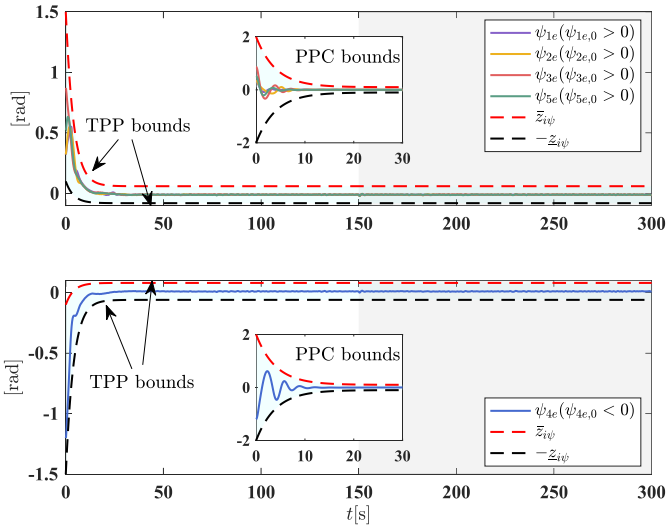

Fig. 6. The heading errors under proposed TPP constraint and standard PPC constraint proposed in [18].

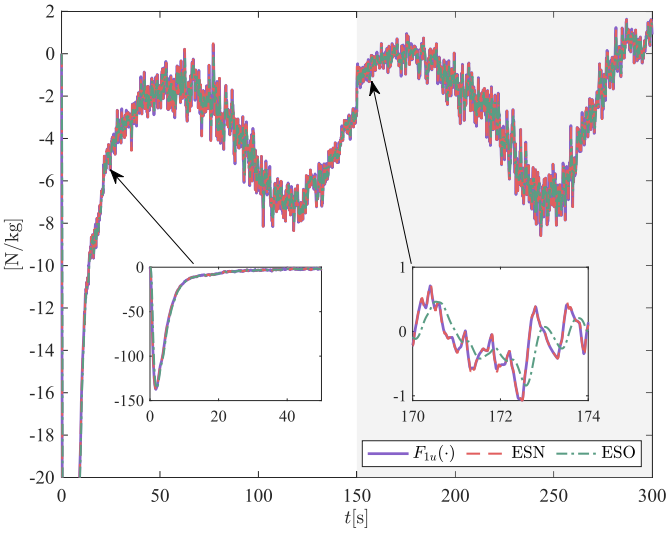

Fig. 7. The estimation property for the total surge disturbances with ESN-based estimators and ESO proposed in [55].

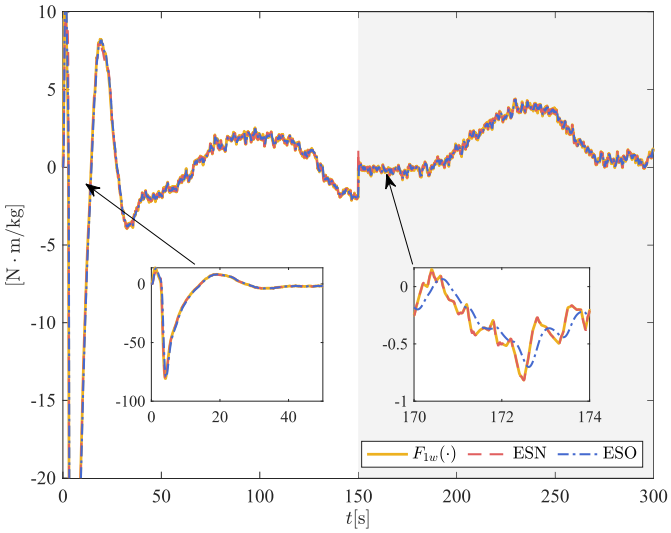

Fig. 8. The estimation property for the total surge disturbances with ESN-based estimators and ESO proposed in [55].

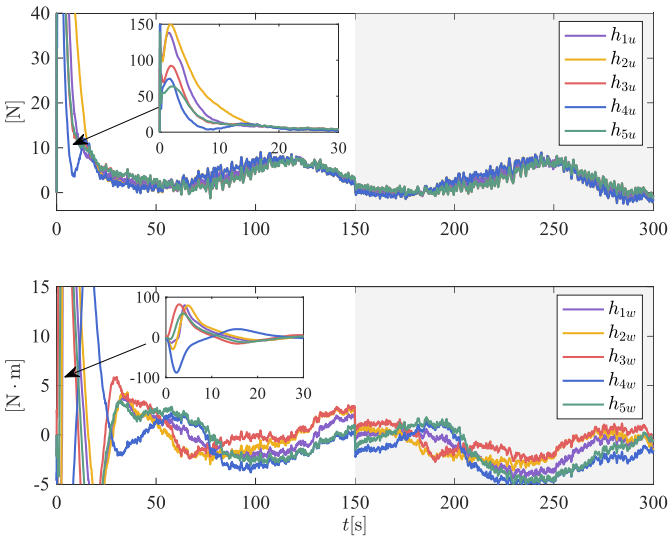

Fig. 9. The desired surge forces and yaw moments of five MSVs.

$\boldsymbol{\eta}_4(0) = [-15, 20, 0]^T$, and $\boldsymbol{\eta}_5(0) = [-15, -15, 0]^T$. The model parameters of MSVs can be found in literature [40] for further details. For brevity and convenience, TABLE I lists the parameters for TPP constraints (6)-(8), the tunnel guidance law (16), the reservoir (21), the ESN-based neural estimator (22), the adaptive law (23), and the control law (26). Herein, nine neurons for ESNs (21) are used in the hidden layer, and activation function is set as $1/(1+e^{-x})$. Consider the fault parameters $\gamma_{iu} = 1 - 0.6|\sin(0.02\ t)|$, $\gamma_{iw} = 1 - 0.2|\sin(0.02\ t)|$, and

$$\begin{aligned} \tau_{iu}^f &= \begin{cases} 1.6|\sin(0.02(t-200))|, & t \geq 150 \\ 0, & \text{others}, \end{cases} \\ \tau_{iw}^f &= \begin{cases} 2.2|\sin(0.02(t-200))|, & t \geq 150 \\ 0, & \text{others}. \end{cases} \end{aligned} \tag{49}$$

In this simulation, the PPC method proposed in [18] is used to demonstrate the superiority of our proposed method. Simulation results are plotted in Figs. 4-9, where the grey background area indicates the fault period of actuator. Fig. 4 draws the actual trajectories of five underactuated MSVs using proposed ESN-based transient-reinforced tunnel coordinated control method. Fig. 4 also displays the formation snapshots at 0s, 100s, 200s, 300s. According to snapshots, the coordinated formation can follow the reference trajectories from (48) guided by one virtual leader. Figs. 5-6 show the relative distance and heading errors under proposed TPP and standard PPC constraints. It is seen from Fig. 5 that errors $E_1,\ldots,E_5$ evolve within the TPP and PPC bounds with the similar shapes due to non-negative definition of E_i. As shown in Fig. 6, the overshoot of heading tracking errors with the TPP constraints can be reduced comparing to the PPC method in [18]. Besides, the tracking errors still evolve within the TPP constraints regardless of actuator faults defined by (49). Figs. 7-8 show the estimation performance of neural estimators (22) for unknown functions with comparison from

extended state observer (ESO) proposed in [55]. From the enlarged curves of Figs. 7-8, the presented ESN-based estimators (22) can more precisely recover the unknown functions $F_{iu}(\cdot)$ and $F_{iw}(\cdot)$ including actuator faults under unknown variables γ_{iu} and γ_{iw}. Fig. 8 depicts the desired control signals of five MSVs in the presence of unknown actuator faults. At 150s, the desired surge forces τ_{iu}^s and yaw moments τ_{iw}^s adjust rapidly due to additive faults in execution.

VI. Conclusion

In this paper, an ESN-based transient-reinforced tunnel coordination control method has been proposed for multiple underactuated MSVs subject to internal uncertainties, external disturbances, and actuator faults. Various coordination patterns of MSVs can be achieved by only redesigning the graph-based trajectory generator. The TPP-constrained coordination of underactuated MSVs has a smaller transient overshoot and higher state-steady accuracy. Then, the presented ESN-based surge and yaw control laws can force the tracking errors to evolve within the TPP regions even in the presence of actuator faults. The boundedness of all error signals are ensured via the input-to-state stability and cascade stability theory. Comparison simulation results verified the effectiveness and superiority of the proposed method. In the future, it is desirable to perform the prescribed performance coordination of underactuated MSVs subject to actuator faults and environmental obstacles.

References

[1] N. Gu, D. Wang, Z. Peng, J. Wang, and Q.-L. Han, "Advances in line-of-sight guidance for path following of autonomous marine vehicles: An overview," *IEEE Trans. Syst. Man, Cybern. Syst.*, vol. 53, no. 1, pp. 12–28, Jan. 2023.

[2] G. Zhang, S. Liu, X. Zhang, and W. Zhang, "Event-triggered cooperative formation control for autonomous surface vehicles under the maritime search operation," *IEEE Trans. Intell. Transp. Syst.*, vol. 23, no. 11, pp. 21392–21404, Nov. 2022.

[3] Y. Shi, C. Shen, H. Fang, and H. Li, "Advanced control in marine mechatronic systems: A survey," *IEEE/ASME Trans. Mechatronics*, vol. 22, no. 3, pp. 1121–1131, Jun. 2017.

[4] W. Wu, Z. Peng, D. Wang, L. Liu, and Q.-L. Han, "Network-based line-of-sight path tracking of underactuated unmanned surface vehicles with experiment results," *IEEE Trans. Cybern.*, vol. 52, no. 10, pp. 10937–10947, Oct. 2022.

[5] W. Tao et al., "Coordination and optimization control framework for vessels platooning in inland waterborne transportation system," *IEEE Trans. Intell. Transp. Syst.*, early access, Nov. 11, 2022, doi: 10.1109/TITS.2022.3220000.

[6] X. Hu, G. Zhu, Y. Ma, Z. Li, R. Malekian, and M. Á. Sotelo, "Event-triggered adaptive fuzzy setpoint regulation of surface vessels with unmeasured velocities under thruster saturation constraints," *IEEE Trans. Intell. Transp. Syst.*, vol. 23, no. 8, pp. 13463–13472, Aug. 2022.

[7] B. Du, B. Lin, C. Zhang, B. Dong, and W. Zhang, "Safe deep reinforcement learning-based adaptive control for USV interception mission," *Ocean Eng.*, vol. 246, Feb. 2022, Art. no. 110477.

[8] W. Wu, Y. Zhang, W. Zhang, and W. Xie, "Distributed finite-time performance-prescribed time-varying formation control of autonomous surface vehicles with saturated inputs," *Ocean Eng.*, vol. 266, Dec. 2022, Art. no. 112866, doi: 10.1016/j.oceaneng.2022.112866.

[9] Z. Peng, D. Wang, T. Li, and M. Han, "Output-feedback cooperative formation maneuvering of autonomous surface vehicles with connectivity preservation and collision avoidance," *IEEE Trans. Cybern.*, vol. 50, no. 6, pp. 2527–2535, Jun. 2020.

[10] W. Wu, Y. Zhang, W. Zhang, and W. Xie, "Output-feedback finite-time safety-critical coordinated control of path-guided marine surface vehicles based on neurodynamic optimization," *IEEE Trans. Syst. Man, Cybern. Syst.*, vol. 53, no. 3, pp. 1788–1800, Mar. 2023.

[11] Y. Zhang, W. Wu, and W. Zhang, "Noncooperative game-based cooperative maneuvering of intelligent surface vehicles via accelerated learning-based neural predictors," *IEEE Trans. Intell. Vehicles*, vol. 8, no. 3, pp. 2212–2221, Mar. 2023.

[12] Z. Peng, L. Liu, and J. Wang, "Output-feedback flocking control of multiple autonomous surface vehicles based on data-driven adaptive extended state observers," *IEEE Trans. Cybern.*, vol. 51, no. 9, pp. 4611–4622, Sep. 2021.

[13] Z. Peng, Y. Jiang, L. Liu, and Y. Shi, "Path-guided model-free flocking control of unmanned surface vehicles based on concurrent learning extended state observers," *IEEE Trans. Syst. Man, Cybern. Syst.*, vol. 53, no. 8, pp. 4729–4739, Aug. 2023.

[14] Y. Jiang, Z. Peng, D. Wang, Y. Yin, and Q.-L. Han, "Cooperative target enclosing of ring-networked underactuated autonomous surface vehicles based on data-driven fuzzy predictors and extended state observers," *IEEE Trans. Fuzzy Syst.*, vol. 30, no. 7, pp. 2515–2528, Jul. 2022.

[15] L. Liu, D. Wang, Z. Peng, and Q.-L. Han, "Distributed path following of multiple under-actuated autonomous surface vehicles based on data-driven neural predictors via integral concurrent learning," *IEEE Trans. Neural Netw. Learn. Syst.*, vol. 32, no. 12, pp. 5334–5344, Dec. 2021.

[16] S. Dai, Z. Wu, J. Wang, M. Tan, and J. Yu, "Barrier-based adaptive line-of-sight 3-D path-following system for a multijoint robotic fish with sideslip compensation," *IEEE Trans. Cybern.*, vol. 53, no. 7, pp. 4204–4217, Jul. 2023.

[17] S.-L. Dai, S. He, Y. Ma, and C. Yuan, "Distributed cooperative learning control of uncertain multiagent systems with prescribed performance and preserved connectivity," *IEEE Trans. Neural Netw. Learn. Syst.*, vol. 32, no. 7, pp. 3217–3229, Jul. 2021.

[18] Z. Jia, Z. Hu, and W. Zhang, "Adaptive output-feedback control with prescribed performance for trajectory tracking of underactuated surface vessels," *ISA Trans.*, vol. 95, pp. 18–26, Dec. 2019.

[19] L. Chen, R. Cui, C. Yang, and W. Yan, "Adaptive neural network control of underactuated surface vessels with guaranteed transient performance: Theory and experimental results," *IEEE Trans. Ind. Electron.*, vol. 67, no. 5, pp. 4024–4035, May 2020.

[20] S.-L. Dai, M. Wang, and C. Wang, "Neural learning control of marine surface vessels with guaranteed transient tracking performance," *IEEE Trans. Ind. Electron.*, vol. 63, no. 3, pp. 1717–1727, Mar. 2016.

[21] Z. Zheng and M. Feroskhan, "Path following of a surface vessel with prescribed performance in the presence of input saturation and external disturbances," *IEEE/ASME Trans. Mechatronics*, vol. 22, no. 6, pp. 2564–2575, Dec. 2017.

[22] H. Wang, M. Li, C. Zhang, and X. Shao, "Event-based prescribed performance control for dynamic positioning vessels," *IEEE Trans. Circuits Syst. II, Exp. Briefs*, vol. 68, no. 7, pp. 2548–2552, Jul. 2021.

[23] B. S. Park and S. J. Yoo, "Robust trajectory tracking with adjustable performance of underactuated surface vessels via quantized state feedback," *Ocean Eng.*, vol. 246, Feb. 2022, Art. no. 110475.

[24] J. Li, X. Xiang, and S. Yang, "Robust adaptive neural network control for dynamic positioning of marine vessels with prescribed performance under model uncertainties and input saturation," *Neurocomputing*, vol. 484, pp. 1–12, May 2022, doi: 10.1016/j.neucom.2021.03.136.

[25] J.-X. Zhang and T. Chai, "Singularity-free continuous adaptive control of uncertain underactuated surface vessels with prescribed performance," *IEEE Trans. Syst. Man, Cybern. Syst.*, vol. 52, no. 9, pp. 5646–5655, Sep. 2022.

[26] N. Wang, Y. Gao, and X. Zhang, "Data-driven performance-prescribed reinforcement learning control of an unmanned surface vehicle," *IEEE Trans. Neural Netw. Learn. Syst.*, vol. 32, no. 12, pp. 5456–5467, Dec. 2021.

[27] Z. Peng, J. Wang, D. Wang, and Q.-L. Han, "An overview of recent advances in coordinated control of multiple autonomous surface vehicles," *IEEE Trans. Ind. Informat.*, vol. 17, no. 2, pp. 732–745, Feb. 2021.

[28] J. Zhang and G. Yang, "Fault-tolerant leader-follower formation control of marine surface vessels with unknown dynamics and actuator faults," *Int. J. Robust Nonlinear Control*, vol. 28, no. 14, pp. 4188–4208, Sep. 2018.

[29] S. He, M. Wang, S.-L. Dai, and F. Luo, "Leader–follower formation control of USVs with prescribed performance and collision avoidance," *IEEE Trans. Ind. Informat.*, vol. 15, no. 1, pp. 572–581, Jan. 2019.

[30] S.-L. Dai, S. He, H. Cai, and C. Yang, "Adaptive leader–follower formation control of underactuated surface vehicles with guaranteed performance," *IEEE Trans. Syst. Man, Cybern. Syst.*, vol. 52, no. 3, pp. 1997–2008, Mar. 2022.

[31] B. S. Park and S. J. Yoo, "Connectivity-maintaining and collision-avoiding performance function approach for robust leader–follower formation control of multiple uncertain underactuated surface vessels," *Automatica*, vol. 127, May 2021, Art. no. 109501.

[32] J. Ghommam, M. Saad, and F. Mnif, "Prescribed performances based fuzzy-adaptive output feedback containment control for multiple underactuated surface vessels," *Ocean Eng.*, vol. 249, Apr. 2022, Art. no. 110898.

[33] Y. Lu, X. Xu, L. Qiao, and W. Zhang, "Robust adaptive formation tracking of autonomous surface vehicles with guaranteed performance and actuator faults," *Ocean Eng.*, vol. 237, Oct. 2021, Art. no. 109592.

[34] S.-L. Dai, S. He, H. Lin, and C. Wang, "Platoon formation control with prescribed performance guarantees for USVs," *IEEE Trans. Ind. Electron.*, vol. 65, no. 5, pp. 4237–4246, May 2018.

[35] S.-L. Dai, S. He, Y. Ma, and C. Yuan, "Cooperative learning-based formation control of autonomous marine surface vessels with prescribed performance," *IEEE Trans. Syst. Man, Cybern. Syst.*, vol. 52, no. 4, pp. 2565–2577, Apr. 2022.

[36] L.-Y. Hao, H. Zhang, H. Li, and T.-S. Li, "Sliding mode fault-tolerant control for unmanned marine vehicles with signal quantization and time-delay," *Ocean Eng.*, vol. 215, Nov. 2020, Art. no. 107882.

[37] Z.-Q. Liu, Y.-L. Wang, and Q.-L. Han, "Adaptive fault-tolerant trajectory tracking control of twin-propeller non-rudder unmanned surface vehicles," *Ocean Eng.*, vol. 285, Oct. 2023, Art. no. 115294.

[38] W. Wu, D. Wu, Y. Zhang, S. Chen, and W. Zhang, "Safety-critical trajectory tracking for mobile robots with guaranteed performance," *IEEE/CAA J. Autom. Sinica*, Aug. 2023, doi: 10.1109/JAS.2023.123864.

[39] Y. Zhang, D. Wang, Y. Yin, and Z. Peng, "Event-triggered distributed coordinated control of networked autonomous surface vehicles subject to fully unknown kinetics via concurrent-learning-based neural predictor," *Ocean Eng.*, vol. 234, Aug. 2021, Art. no. 108966.

[40] T. I. Fossen, *Handbook of Marine Craft Hydrodynamics and Motion Control*. Hoboken, NJ, USA: Wiley, 2011.

[41] R. Ji, B. Yang, J. Ma, and S. S. Ge, "Saturation-tolerant prescribed control for a class of MIMO nonlinear systems," *IEEE Trans. Cybern.*, vol. 52, no. 12, pp. 13012–13026, Dec. 2022.

[42] Z. Peng, D. Wang, Z. Chen, X. Hu, and W. Lan, "Adaptive dynamic surface control for formations of autonomous surface vehicles with uncertain dynamics," *IEEE Trans. Control Syst. Technol.*, vol. 21, no. 2, pp. 513–520, Mar. 2013.

[43] L. Liu, D. Wang, Z. Peng, C. L. P. Chen, and T. Li, "Bounded neural network control for target tracking of underactuated autonomous surface vehicles in the presence of uncertain target dynamics," *IEEE Trans. Neural Netw. Learn. Syst.*, vol. 30, no. 4, pp. 1241–1249, Apr. 2019.

[44] X. Jin, "Fault tolerant finite-time leader–follower formation control for autonomous surface vessels with LOS range and angle constraints," *Automatica*, vol. 68, pp. 228–236, Jun. 2016.

[45] X. Hu, X. Wei, Y. Kao, and J. Han, "Robust synchronization for underactuated vessels based on disturbance observer," *IEEE Trans. Intell. Transp. Syst.*, vol. 23, no. 6, pp. 5470–5479, Jun. 2022.

[46] R. P. Paul, *Robot Manipulators: Mathematics, Programming, and Control: the Computer Control of Robot Manipulators*. Los Angeles, CA, USA: Richard Paul, 1981.

[47] N. Gu, Z. Peng, D. Wang, Y. Shi, and T. Wang, "Antidisturbance coordinated path following control of robotic autonomous surface vehicles: Theory and experiment," *IEEE/ASME Trans. Mechatronics*, vol. 24, no. 5, pp. 2386–2396, Oct. 2019.

[48] W. Wu, Z. Peng, D. Wang, L. Liu, and N. Gu, "Anti-disturbance leader–follower synchronization control of marine vessels for underway replenishment based on robust exact differentiators," *Ocean Eng.*, vol. 248, Mar. 2022, Art. no. 110686.

[49] S.-L. Dai, S. He, H. Cai, and C. Yang, "Adaptive leader-follower formation control of underactuated surface vehicles with guaranteed performance," *IEEE Trans. Syst. Man, Cybern. Syst.*, vol. 52, no. 3, pp. 1997–2008, Mar. 2022.

[50] R. Ji, D. Li, J. Ma, and S. S. Ge, "Saturation-tolerant prescribed control of MIMO systems with unknown control directions," *IEEE Trans. Fuzzy Syst.*, vol. 30, no. 12, pp. 5116–5127, Dec. 2022.

[51] Z. Peng, J. Wang, and D. Wang, "Containment maneuvering of marine surface vehicles with multiple parameterized paths via spatial–temporal decoupling," *IEEE/ASME Trans. Mechatronics*, vol. 22, no. 2, pp. 1026–1036, Apr. 2017.

[52] G. Zhu, Y. Ma, Z. Li, R. Malekian, and M. Sotelo, "Dynamic event-triggered adaptive neural output feedback control for MSVs using composite learning," *IEEE Trans. Intell. Transp. Syst.*, vol. 24, no. 1, pp. 787–800, Jan. 2023.

[53] G. Zhu, Y. Ma, Z. Li, R. Malekian, and M. Sotelo, "Event-triggered adaptive neural fault-tolerant control of underactuated MSVs with input saturation," *IEEE Trans. Intell. Transp. Syst.*, vol. 23, no. 7, pp. 7045–7057, Jul. 2022.

[54] H. K. Khalil, *Nonlinear Control*. London, U.K.: Pearson, 2015.

[55] L. Liu, D. Wang, and Z. Peng, "ESO-based line-of-sight guidance law for path following of underactuated marine surface vehicles with exact sideslip compensation," *IEEE J. Ocean. Eng.*, vol. 42, no. 2, pp. 477–487, Apr. 2017.

Wentao Wu (Graduate Student Member, IEEE) received the B.E. degree in electrical engineering and automation from the Harbin University of Science and Technology, Harbin, China, in 2018, and the M.E. degree in electrical engineering from Dalian Maritime University, Dalian, China, in 2021. He is currently pursuing the Ph.D. degree in electronic information with Shanghai Jiao Tong University, Shanghai, China.

His current research interests include cooperative control, safety-critical control, and constrained control of multiple marine vehicles.

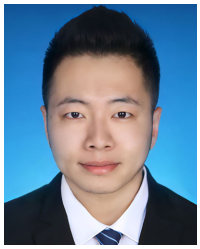

Ruihang Ji (Member, IEEE) received the B.S. and Ph.D. degrees in control science and engineering from the Harbin Institute of Technology, China, in 2016 and 2021, respectively.

He was a joint Ph.D. Student supported by the China Scholarship Council with the Department of Electrical and Computer Engineering, National University of Singapore, where he is currently a Research Fellow. His current research interests include nonlinear control, unmanned systems, and human–robot interaction.

Weidong Zhang (Senior Member, IEEE) received the B.S., M.S., and Ph.D. degrees from Zhejiang University, Hangzhou, China, in 1990, 1993, and 1996, respectively.

He was a Post-Doctoral Fellow with Shanghai Jiao Tong University, Shanghai, China, where he joined as an Associate Professor in 1998 and has been a Full Professor since 1999. From 2003 to 2004, he was with the University of Stuttgart, Stuttgart, Germany, as an Alexander von Humboldt Fellow. He is currently the Director of the Engineering Research Center of Marine Automation, Shanghai Municipal Education Commission, and the Director of the Marine Intelligent System Engineering Research Center, Ministry of Education, China. He is the author of 265 SCI papers and one book and holds 72 patents. His research interests include control theory, machine learning theory, and their applications in industry and autonomous systems. He was a recipient of the National Science Fund for Distinguished Young Scholars, China, and the Cheung Kong Scholar, Ministry of Education.

Yibo Zhang (Member, IEEE) received the B.E. degree in marine electronic and electrical engineering and the Ph.D. degree in marine electrical engineering from Dalian Maritime University, Dalian, China, in 2014 and 2021, respectively.

He is currently a Post-Doctoral Fellow with the Department of Automation, Shanghai Jiao Tong University. His current research interests include cooperative control and intelligent control of multi-agent systems and multiple marine vehicles.